Investigation of Turn Number of the Coil on Tube Forming Performance in Electromagnetic Pulse Forming

Xianmin Wang[1]*, Chengxiang Li[1], Yan Zhou[1], Jian Du[2], Zhigang Liao[2]

[1] State Key Laboratory of Power Transmission Equipment and System Security and New Technology, School of Electrical Engineering, Chongqing University, Chongqing, 400044 China
[2] State Grid Chongqing Electric Power Company Yongchuan Power Supply Branch, Chongqing, 402160, China
*Corresponding author. Email: wangxianmin@cqu.edu.cn

Abstract

Electromagnetic pulse forming (EMPF) is an environmentally friendly and high-speed forming method without pollution generating. As the key component for energy conversion, the coil has a significant influence on the forming performance. Consequently, this paper aims to study the effect of the turn number of the coil on the performance of the tube forming through the theoretical analysis model and experiments. Based on the connection among the electrical parameters of the coil, the current parameters of the discharge pulse, and electromagnetic force, a theoretical model is built to analyze the qualitative connection between the number of turns of the coil and the amount of forming. Then, the EMPF experiments with the same discharge energy of 3.4kJ are carried out to verify the established model through the established EMPF equipment. The experimental results are consistent with the theoretical analysis. The results show that the peak value of the current amplitude and rise time of the pulse decrease respectively with the increase of the number of turns of the coil because the increments of the number of turns lead to the rising coil inductance. But the forming amount of the tube increases first and then decreases. So there is an optimal value of the turn number for the coil to generate the maximum Lorentz force to deform the workpiece. Therefore, it is worthwhile to choose the proper number of coil turn to improve the effect of EMPF.

Keywords

Magnetic pulse forming, Coil, Turn number

1 Introduction

Metal materials are widely used in the fields of the automotive industry, aerospace industry, military manufacturing, and other industries, as Kapil and Abhay (2015) reported. Electromagnetic pulse forming (EMPF) is a metal fabrication processing approach that utilizes the storage and release of charge to deform metal materials. This technique enables to overcome challenges as energy shortage and control of pollution. Psyk et al. (2011) reveal that hardly is any greenhouse gas, radiation, hazardous substance, or smoke generated within the EMPF, so it is evident to notice promising potentials of EMPF for its environmentally friendly operation.

These advantages have motivated a comprehensive investigation to obtain a more profound understanding and feasible application. Raoelison et al. (2013) built up a weldability window that includes the collision velocity and angle. L'Eplattenier and I. (2016) established a coupled model between 2D and 3D to speed up the simulation. The influence of temperature rise, discharge frequency, and material properties of the surface on EMPF is verified by Zhou et al. (2018), Lueg-Althoff et al. (2018), and Cui et al. (2018) respectively. In the process of EMPF, a large current flows through the loop and induces an electromagnetic field in the coil. The electromagnetic force is generated by the current induced on the time-varying electromagnetic field object. Then the electromagnetic force makes the object deform and energy mainly releases on the coil in the circuit. It is remarkable that the coil is the key component for energy conversion and needs to be optimized.

In the research of EMPF coils, Cao et al. (2015) used a crowbar circuit, controlling the discharge current in the coil to decrease the Joule heating. This reduces the temperature rising of the coil winding. A multi-layer coil was designed by Luo et al. (2014) for sheet forming based on analyzing the effect of the coil structure on the magnetic field and forming amount. To further decrease the mechanical stress of the coil, Li et al. (2020) proposed a background magnetic field to enhance the forming force and designed a dual-coil EMF system to generate a background magnetic field for tube forming. Conway and John (2010) analyzed the coil with a rectangular cross-section and presented a method to calculate the inductance of this kind of coil by using Bessel and Struve functions. Relevant research in the structure parameters and assembly optimization for forming coil was performed by Zhu (2018) and Zhang (2017). Ahmed et al. (2011) proposed a method to design the coil based on FEM. However, in previous studies on pulse forming, the analytical basis mainly focuses on the metal material characteristics after forming. Furthermore, the number of turns of the coil in those researches was simply emphasized and few researchers proposed systematic analysis and research about coil turn. Instead, the number of coil turn is just simply informed

without comprehensive and convincing reasons. Rare research focuses on the relationship between the coil turns and forming effect.

In the work of this paper, we implement EMPF experiments by coils with different turn numbers to figure out the forming effect of the turn number of the coil on tube forming performance. Those coils are equipped with the same field shaper and loaded with unvaried work areas under constant input energy. In other words, the winding area is unaltered, only the turn number of the coil varies. Simulation models are built to figure out the optimal parameters which help generate the maximum Lorentz force. This paper highlights the effects of the turns of the coil on the EMPF process. Additionally, we analyze the influence of the number of coil turn on other parameters, such as inductance, peak amount, and rising time of the pulse current. Under the same input energy condition, the effect of pulse forming first increases and then decreases with the increase of the turn number, and there is an optimized coil turns to maximize the forming amount, thus significantly improving the energy utilization rate.

2 Theoretical Analysis

2.1 Circuit model

EMPF process could be summarized as the rapidly violent release of energy. Specifically, the energy is stored by charging the capacitor bank for a long period and then hastily released to a coil by triggering the switch within several hundred μs. The equivalent circuit of the EMPF system is shown in Fig. 1. L_c and R_c are the resistance and inductance of the coil respectively. L_m and R_m are the inductance and resistance in the capacitor discharge circuit respectively. Similarly, L_w and R_w are the inductance and resistance of the working part respectively, as shown in Thibaudeau and Brad (2015).

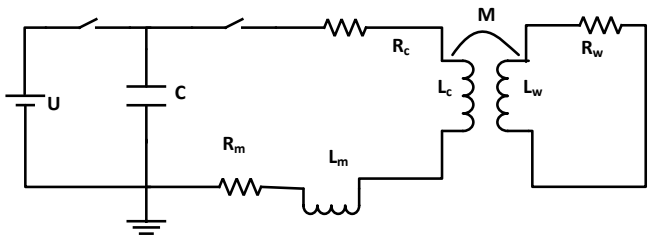

***Figure 1**: Diagram of the equivalent circuit*

Since mutual inductance exists, the value of mutual inductance can be calculated as:

$$M = k\sqrt{L_c L_w} \tag{1}$$

Where k denotes the mutual inductance coefficient, reflecting the flux of two coils. k is equal from 0 to 1. Generally speaking, the mutual inductance coefficient can be directly measured in the experimental results. It equals the ratio of the current on the capacitor side to the

current on the forming object. In this paper, we take into account that the connection between the object and the coil is close enough. That is, all magnetic flux in the tube passes through the load. The skin effect is taken into account when the current waveform oscillates. This effect depth is calculated according to **Eq. 2**.

$$\delta = \sqrt{\frac{2\rho}{\mu_r \mu_0 \omega}} \tag{2}$$

Where δ, μ_0, μ_r, ρ_0, and ω are the skin depth, the vacuum permeability, the relative permeability, the conductor resistivity, and the angular frequency of current respectively. **Eq. 2** reflects the inhomogeneity of the alternative current distribution inside the conductor. Known skin depth, according to Nassiri et al. (2015), the coil resistance should be calculated as **Eq. 3** because the skin effect increases the resistance of the circuit.

$$R_c = \rho_0 \frac{p}{A_{eff}} \tag{3}$$

Where p and A_{eff} denote the length of the coil and the sectional area respectively. The inductance of the coil is:

$$L_c = \frac{KL\mu n^2}{S} \tag{4}$$

Where *K*, *n*, *S*, and *L* represent the Long Beam coefficient, the number of the coil turns, the sectional area of the coil winding, and the length of the coil respectively. The cross-sectional area is the ring from the skin depth to the coil surface, so we sum up resistance and inductance of the whole circuit respectively as

$$R = R_c + R_m, \qquad L = L_c + L_m \tag{5}$$

In **Eq. 5**, *R*, R_m, and R_c denote the sum resistance, circuit resistance, and coil resistance respectively. Similar to *L*, L_m and *L*c. Kirchhoff's voltage law (KVL) could be applied in this circuit within the discharge process, and then the state equation of the second-order circuit is listed as

$$\frac{1}{C}\int i dt + iR + L\frac{di}{dt} = 0 \tag{6}$$

Where *i* and C denote the current flowing through the coil and the sum capacitance of the circuit. In the beginning, assuming that the current is 0 and the gradient of current is:

$$i(0) = 0, \qquad \frac{di}{dt}(0) = \frac{U}{L} \tag{7}$$

Where U is the voltage charging on the capacitor bank. Thus, the current **Eq. 6** can be solved as:

$$i(t) = \frac{U}{\sqrt{1-\alpha^2}}\sqrt{\frac{C}{L}}e^{-\alpha\omega t}sin\omega\sqrt{1-\alpha^2}t \tag{8}$$

Where ω and α are calculated as:

$$\omega = \frac{1}{\sqrt{LC}}, \qquad \alpha = \frac{R}{2}\sqrt{\frac{C}{L}} \tag{9}$$

2.2 Electromagnetic Field and Mechanical theory

The current flowing through the coil will produce electromagnetic fields. Maxwell's equations can be applied to express the series characteristics.

$$\nabla \times \vec{H} = \vec{J} + \frac{\partial \vec{D}}{\partial t} \tag{10}$$

$$\nabla \times \vec{E} = -\frac{\partial \vec{B}}{\partial t} \tag{11}$$

$$\nabla \cdot \vec{B} = 0 \tag{12}$$

$$\sigma_s \vec{E} = \vec{J} \tag{13}$$

Where the magnetic field intensity $\vec{H}$, the electric displacement vector $\vec{D}$, the surface current density $\vec{J}$, the magnetic induction intensity $\vec{B}$ and the electric field intensity $\vec{E}$ are related to each other. These equations demonstrate that conducting a current or time-varying electric field can generate a magnetic field and vice versa.

It should be pointed out that displacement current($\frac{\partial \vec{D}}{\partial t}$) is negligible in the low-frequency electromagnetic field Zhu (2018), so **Eq. 10** above is modified as

$$\nabla \times \vec{H} = \vec{J} \tag{14}$$

As for multi-turns coil, based on the section diagram of forming assembly (**Fig.2**), the relationship among H, i, and n are expressed as follows according to Manoharan et al. (2013).

$$H \propto \mathrm{ni} \tag{15}$$

Where H is the amplitude of magnetic field intensity and n is the turn number of the coil. According to **Eq.14** and **Eq. 15**, the current density amplitude of the tube is also relevant to the coil current.

$$\mathrm{J} \propto \frac{\partial \varphi}{\partial t} \propto \mathrm{n}\frac{\partial \mathrm{i}}{\partial t} \tag{16}$$

As a result, the current induced by the time-varying electromagnetic field on the object will generate a Lorentz force in the magnetic field. The Lorentz force can be expressed as **Eq.17**:

$$\vec{F} = \vec{J} \times \vec{B} = |J| \cdot |B| \cdot sin\theta \cdot \vec{e}^{F} \tag{17}$$

Where θ, $\vec{e}^{F}$ are the angle between $\vec{J}$ and $\vec{B}$, the unit direction vector of the Lorentz force respectively. So the force amplitude is relevant to the number of turns of the coil.

$$\mathrm{F} \propto n^2 \cdot i \cdot \frac{\partial \mathrm{i}}{\partial t} \tag{18}$$

When the Lorentz force is large enough to deform the tube. The deformation formula is shown in **Eq. 19**.

$$\vec{F} = \rho \frac{\partial^2 \vec{S}}{\partial t^2} - \nabla \cdot \sigma \tag{19}$$

Where $\vec{S}$, ρ and σ symbolize the displacement of the tube, the metal density, and the flow strength respectively. The first turn on the right side of this equation represents Newton's Second Law.

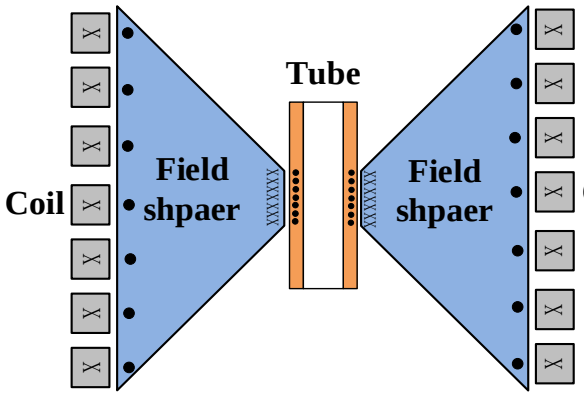

***Figure 2**: Section diagram of forming assembly and current density distribution*

3 Numerical Simulation and Experiments

In this paper, we analyze the effect of coil parameters on the maximum forming force by building an axisymmetric 2D finite element model in COMSOL Multiphysics. The geometry model and grid generation are shown in **Fig. 3(a)** and **Fig. 3(b)** respectively. The control

equations have been listed in part 2. The magnetic field module and the solid mechanics module are coupled through **Eq. 17** and **Eq. 19**.

Firstly, the relevant parameters' values of the circuit elements (except the coil) are measured by the RLC digital electric bridge. These parameters include capacitance (C), resistance (R_m), and inductance of the circuit (L_m). Then, based on **Eq. 3** and **Eq. 4**, the coil inductance (L_c) and resistance (R_c) can be calculated through the number of coil turns (n). Then the mutual inductance coefficient is calculated through measurement. Next, the total inductance value (L) and the total resistance value (R), which is obtained by adding the inductance value of the other parts of the loop, are substituted into the calculation of the loop current function. Then the loop current is substituted to the coil in the finite element model to compute the process.

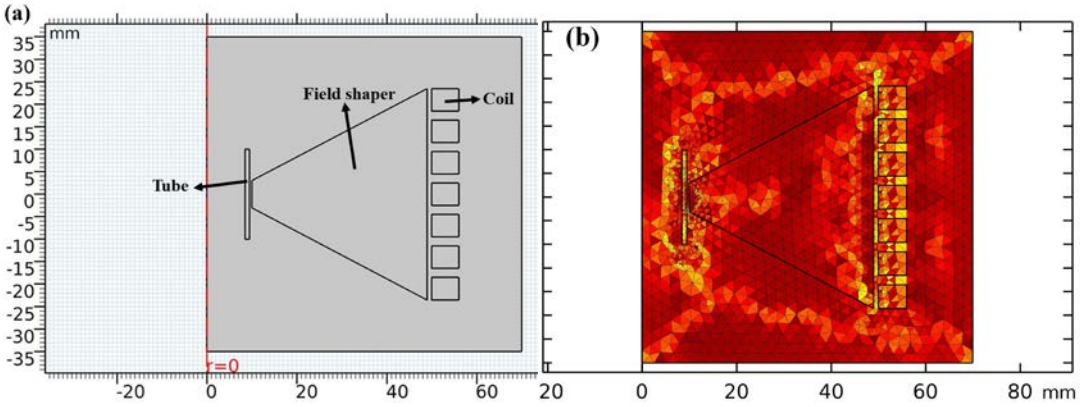

***Figure 3**: Finite element model (a) geometry model (b) grid*

The electromagnetic pulse forming system consists of three modules: energy storage module, energy load module, and switch. The energy storage system consists of nine capacitors in parallel, which is equivalent to 135μF. The maximum DC voltage that each capacitor can withstand is 25kV with a maximum peak current of 220kA. And the stray inductance is less than 60nH. The energy release module is a coil with a field shaper, which needs to be loaded with pipe fittings when forming. To minimize the resistance in the circuit, the chosen materials are copper. The switch module is composed of a trigger vacuum switch (TVS) controlled by an FPGA. The principle diagram of the whole system is shown in **Fig. 4 (a)**.

Considering that the trigger voltage of TVS is 5kV, we divide the trigger module into two modules: the FPGA control part and the electrical module. Those two modules can generate the voltage signal to trigger the TVS. Besides, the control module and the electrical module cannot withstand a high pulse voltage. Two isolation topology is established to ensure the security of these modules.

As for the charging power supply, a high-voltage DC power supply is utilized to charge the capacitor bank. A vacuum relay is added between the power supply and capacitor to ensure the security of the circuit. The experimental platform is set up as shown in **Fig. 4(b)**. As for signal acquisition, the Rogowski coil is used to measure the current.

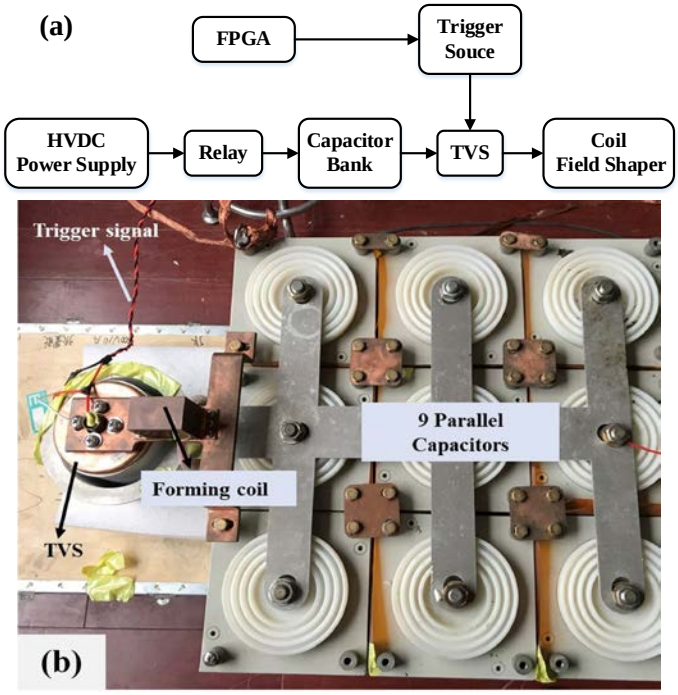

***Figure 4**: Diagram of the system (a) Principle (b) Equipment*

4 Results and Discussion

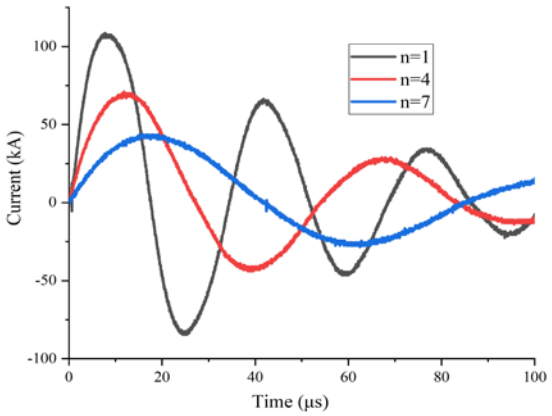

***Figure 5**: Current waveform of different turn numbers of coil*

The curves in **Fig. 5** show the current waveforms flowing through coils with different turns. The obvious decline tendency of the current amplitude and frequency is observed when the number of turns is reinforced. Specifically, the peak current flowing through the 1-turn, 4-turn, and 7-turn coil with load is about 105kA, 65kA, 40kA respectively, and the half-peak period is about 17μs, 27μs, and 42μs respectively. **Fig. 6** shows the relationship between the maximum Lorentz force and the number of turns of the coil. With the increase of the number

of turns, the force first enhances and then reduces, accompanied by a maximum value. The number of turns corresponding to its maximum value is about 11. When the turns reach maximum, force reduction will occur with turns continuously escalating.

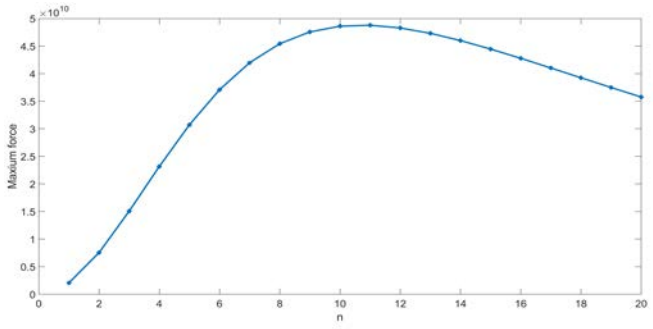

***Figure 6**: Results of the force under different turn numbers of coil*

The experimental deformation results are shown in **Fig. 7(b)**. It is noticeable that the remarkably diverse deformation exists with the coil turns increasing under the same input energy. There is no noticeable deformation area when the turn number is less than 4. The experimental deformation shape is consistent with the simulation results in **Fig.7(a)**.

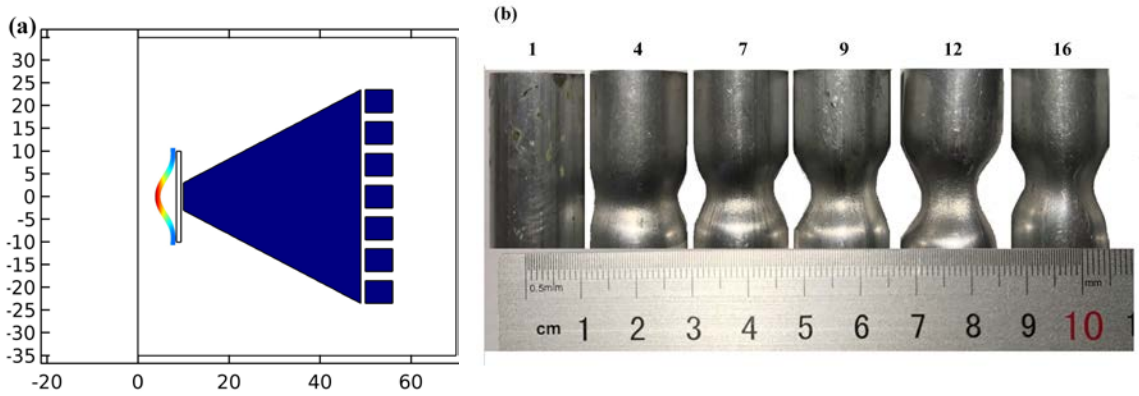

***Figure 7**: Forming Results (a) simulation (b) experiment*

Furthermore, the deformation amount measured by the vernier caliper is demonstrated in **Fig. 8**. By comparing the simulation results with the experimental results, we find that the trend of simulated deformation results are in good agreement with the experimental results. The tendency of the forming amount and turn number conforms to a quadratic function. This suggests that there is an optimal turn number of the coil to form the tube.As the number of coil turns increases, the inductance and resistance of the coil will continue to increase, leading to a slow rise of the loop current and a decrease of the current peak. However, the total magnetic flux on the field shpaer increases. According to **Eq. 18,** as long as the product of magnetic flux and magnetic flux change rate increases, the forming effect of the object will increase continuously. When it rises to the optimal value, the product of magnetic flux and the rate of change of magnetic flux begins to decrease, at which time the Lorentz force keeps decreasing.

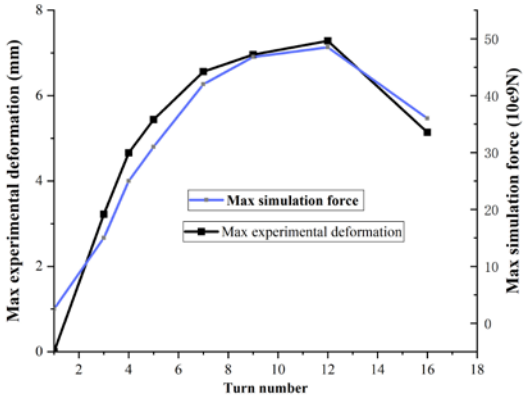

***Figure 8**: Comparison of the experimental forming results and simulation force*

5 Conclusion

In this paper, we study the relationship between the turn number of the coil and the forming effect. Based on theoretical analysis, numerical simulation, and experimental verification, conclusions are drawn as follows.

(1) With the increase of coil turns, the equivalent inductance of the load will increase rapidly. So the Enhancement of inductance significantly leads to the reduction of amplitude and rise time of current in the circuit.

(2) The simulation successfully reproduces the forming shape of the tube. The deformation area mainly focuses on the middle area where the field shaper works on.

(3) There is a quadratic function between the turn number of the coil and the forming effect. This means that the forming effect of coils with different turns increases firstly and then keeps a downward trend. Therefore, there is an optimal number of turns of the coil, which maximizes the forming amount of the coil under the same input energy.

References

Ahmed, M., Panthi, S. K., Ramakrishnan, N., Jha, A. K., Yegneswaran, A. H., Dasgupta, R., & Ahmed, S., 2011. Alternative flat coil design for electromagnetic forming using FEM. Transactions of Nonferrous Metals Society of China, 21(3), pp. 618-625.

Athar, M. H., & Tolaminejad, B., 2015. Weldability window and the effect of interface morphology on the properties of Al/Cu/Al laminated composites fabricated by explosive welding. Materials & Design, 86, pp. 516-525.

Cao, Q., Han, X., Lai, Z., Xiong, Q., Zhang, X., Chen, Q., ... & Li, L. 2015. Analysis and reduction of coil temperature rise in electromagnetic forming. Journal of Materials Processing Technology, 225, 185-194.

Conway, J. T., 2009. Inductance calculations for circular coils of rectangular cross section and parallel axes using Bessel and Struve functions. IEEE Transactions on Magnetics, 46(1), pp. 75-81.

Cui, J., Sun, T., Geng, H., Yuan, W., Li, G., & Zhang, X., 2018. Effect of surface treatment on the mechanical properties and microstructures of Al-Fe single-lap joint by magnetic pulse welding. The International Journal of Advanced Manufacturing Technology, 98(5-8), pp. 1081-1092.

Dond, S., Choudhary, H., Kolge, T., & Sharma, A., 2019. Analysis of the variation of the discharge circuit parameters during electromagnetic forming processes. International Journal of Precision Engineering and Manufacturing, 20(3), pp. 375-382.

Kamal, M., & Daehn, G. S., 2007. A uniform pressure electromagnetic actuator for forming flat sheets. Journal of Manufacturing Science and Engineering 129.2 (2007): pp. 369-379.

Kapil, A., & Sharma, A., 2015. Magnetic pulse welding: an efficient and environmentally friendly multi-material joining technique. Journal of Cleaner Production, 100, pp. 35-58.

L'Eplattenier, P., & Çaldichoury, I., 2016. A coupled 3D/2D axisymmetric method for simulating magnetic metal forming processes in LS-Dyna. In 7th International Conference on High Speed Forming, April 27th-28th 2016, Dortmund, Germany.

Li, X., Cao, Q., Lai, Z., Ouyang, S., Liu, N., Li, M., ... & Li, L. 2020. Bulging behavior of metallic tubes during the electromagnetic forming process in the presence of a background magnetic field. Journal of Materials Processing Technology, 276, 116411.

Lueg-Althoff, J., Bellmann, J., Gies, S., Schulze, S., Tekkaya, A. E., & Beyer, E., 2018. Influence of the flyer kinetics on magnetic pulse welding of tubes. Journal of Materials Processing Technology, 262, pp. 189-203.

Luo, W., Huang, L., Li, J., Liu, X., & Wang, Z. 2014. A novel multi-layer coil for a large and thick-walled component by electromagnetic forming. *Journal of Materials Processing Technology*, *214*(11), 2811-2819.

Manoharan, P., Manogaran, A. P., Priem, D., Marya, S., & Racineux, G., 2013. State of the art of electromagnetic energy for welding and powder compaction. Welding in the World, 57(6), pp. 867-878.

Nassiri, A., Campbell, C., Chini, G., & Kinsey, B., 2015. Analytical model and experimental validation of single turn, axi-symmetric coil for electromagnetic forming and welding. Procedia Manufacturing, 1, pp. 814-827.

Pereira, D., Oliveira, J. P., Pardal, T., Miranda, R. M., & Santos, T. G., 2018. Magnetic pulse welding: machine optimisation for aluminium tubular joints production. Science and Technology of Welding and Joining, 23(2), pp. 172-179.

Psyk, V., Risch, D., Kinsey, B.L., Tekkaya, A.E., Kleiner, M., 2011. *Electromagnetic forming – A review*. Journal of Materials Processing Technology 211 (5), pp. 787-829.

Raoelison, R. N., Buiron, N., Rachik, M., Haye, D., Franz, G., & Habak, M., 2013. Study of the elaboration of a practical weldability window in magnetic pulse welding. Journal of Materials Processing Technology, 213(8), pp. 1348-1354.

Zhu S., 2018. Research on the structure parameters of the coil in the processing of tube electromagnetic forming. M.S. thesis, Dept. Mech. Eng., Shenyang Aerospace Univ., Shenyang, China, 2018.

Thibaudeau, E., & Kinsey, B. L., 2015. Analytical design and experimental validation of uniform pressure actuator for electromagnetic forming and welding. Journal of Materials Processing Technology, 215, pp. 251-263.

Zhang, X., 2017. Numerical Simulation and Experimental Study of Tube Bulging-Drawing Forming under Pulsed High Magnetic Fields. Ph.D. dissertation, Dept. Elect. Eng., Huazhong Univ of Sci and Tech., Wuhan, China, 2017.

Zhou, Y., Tan, J., Yao, C., Li, C., Wang, X., Zhou, W., & Wang, X., 2018. Finite-element simulation and experiments on plastic heating in the process of electromagnetic pulse forming. IEEE Transactions on Plasma Science, 46(10), pp. 3427-3437.